JAAS

ROYAL SOCIETY OF CHEMISTRY

PAPER

View Article Online
View Journal

Cite this: DOI: 10.1039/d5ja00269a

Quantification of the sulfur strand length distribution in organo-sulfur cathode materials with X-ray absorption spectrometry

Konstantin Skudler, *[a] Rukiya Matsidik, [bf] Hongfei Yang, [a] Michael Walter, [cde] Michael Sommer [bf] and Matthias Müller *[a]

Received 9th July 2025
Accepted 29th October 2025

DOI: 10.1039/d5ja00269a

rsc.li/jaas

Lithium–organo-sulfur batteries combine high specific capacities of sulfur-based materials with tunable properties and excellent cycle stability of organic components. The key to designing batteries for specific applications is to understand the correlation between structural and electrochemical properties. The structure of sulfur-containing polymers prepared *via* inverse vulcanization as well as the sulfur load can be tuned by varying the sulfur feed ratio. With a self-absorption corrected linear combination analysis of X-ray absorption spectra, the distribution of sulfur strand lengths is quantitatively determined for double redox-active organo-sulfur networks with varying sulfur loads used as cathode materials in lithium–sulfur batteries.

1 Introduction

Lithium–sulfur batteries are promising candidates for energy storage combining high specific capacity and energy density with the usage of abundant materials.[1–5] However, various degradation mechanisms limit their cycle stability.[6] The effect which is widely considered the most relevant is the so-called polysulfide shuttle.[7] Lithium polysulfides as intermediate products dissolve into the electrolyte and migrate to the anode leading to a loss of active cathode material and rapid capacity fading.[8]

There are several approaches to overcome this polysulfide shuttle effect by the manipulation of the cell. Any such manipulation increasing cycle stability happens at the expense of specific capacity. An ideal cell manipulation therefore retains a high specific capacity while providing increased cycle stability. Besides variations in the electrolyte or the separator,[9,10] a common approach is to adapt the electric and ionic accessibility of sulfur in the cathode.[11]

Organic batteries not only provide environmental and economic benefits, but are also highly tunable and thus offer manifold potential applications.[12–18] They have excellent cycle stability and rate capability, and by incorporating redox-active molecules into a polymer network, their mechanical and electrochemical properties can be adapted to various required applications.[12,16–22]

Hybrid organo-sulfur batteries are a promising approach to increase the cycle stability of sulfur-based batteries.[23] Organic polymers can be used to confine sulfur within the cathode region due to their porous structures.[24] However, sulfur can also be utilized to crosslink monomer units into organo-sulfur polymer networks *via* covalent C–S bonds.[23,25] In this way, the specific capacity significantly increases compared to pure organic batteries while the cycle stability increases because of the hindered polysulfide shuttle.

Recently, a double redox-active organo-sulfur polymer network using a naphthalene diimide (NDI) core as a crosslinker was presented as a cathode material.[26] By varying the sulfur feed ratio in Inverse Vulcanization (IV), the sulfur strand length and subsequently the electrochemical properties of the resulting SNDI cathode networks can be manipulated. In order to tune specific capacity and cycle stability according to certain demands, it is crucial to understand the correlation of the sulfur strand length with both the sulfur feed ratio and the electrochemical properties.

Near Edge X-ray Absorption Fine-Structure (NEXAFS) spectroscopy is an analytical technique to observe unoccupied states in the electronic structure of an element of interest.[27] Depending on various chemical properties such as binding partners, molecule structure and conformation, this electronic structure changes. These changes are qualitatively visible in NEXAFS spectra through shifts in resonance energies and (relative) intensities. NEXAFS has previously been applied to rubber compounds containing sulfur.[28]

By simple analysis of peak intensities after curve fitting of NEXAFS spectra, a value representing the average length of

[a]Physikalisch-Technische Bundesanstalt (PTB), Abbestr. 2-12, 10587 Berlin, Germany. E-mail: Konstantin.Skudler@ptb.de; Matthias.Mueller@ptb.de

[b]Institute for Chemistry, Chemnitz University of Technology, Str. der Nationen 62, 09111 Chemnitz, Germany

[c]Freiburg Center for Interactive Materials and Bioinspired Technologies (FIT), University of Freiburg, Georges-Köhler-Allee 105, 79110 Freiburg, Germany

[d]Cluster of Excellence livMatS @ FIT, Freiburg, Germany

[e]Fraunhofer IWM, MikroTribologie Centrum μTC, Freiburg, Germany

[f]Forschungszentrum MAIN, Chemnitz University of Technology, Rosenbergstraße 6, 09126 Chemnitz, Germany

sulfur strands has been determined.[29] A complementary technique for the quantitative evaluation of NEXAFS spectra used here is the linear combination analysis.

Spectroscopic signatures of organo-sulfur model compounds with well-known sulfur strand lengths were investigated both experimentally and by simulations.[30] The corresponding spectra of different organo-sulfur polymer networks qualitatively suggest structural differences which depend on the sulfur load, leading to a certain incorporated molar ratio of sulfur to monomer units.[26] A network with a low sulfur load features only a few or short sulfur strands, whereas increasing the sulfur feed ratio leads to more and longer sulfur strands. As the exact sulfur strand length is crucial for electrochemical properties such as specific capacity and cycle stability of organo-sulfur cathodes, its distribution needs to be determined quantitatively.

NEXAFS spectra can be analyzed quantitatively by peak fitting or linear combination analysis if they are not damped or distorted, *e.g.* by the self-absorption effect. Battery components consisting of light elements such as sulfur can only be measured in fluorescence mode. In this work, self-absorption free spectra are referred to as spectra with a negligible influence of the self-absorption effect which only applies in the case of extremely thin or diluted samples. However, both the undiluted liquid organo-sulfur molecules and the organo-sulfur cathode materials with relatively high sulfur concentrations and sample thicknesses (liquid film thickness and powder grain size) on the order of at least 1 μm are in a regime where the NEXAFS spectra are affected by self-absorption. Thus, a reliable quantitative analysis of their NEXAFS spectra requires a self-absorption corrected evaluation which is valid for any sample thickness.[31] The utilization of neural networks for reverse mapping between structure and X-ray spectroscopic observables[32] requires large training datasets that consider the self-absorption effect. The combination of linear combination analysis considering the self-absorption effect presented here could enable the application of machine learning models for this purpose.

This work reports self-absorption free NEXAFS spectra of organic mono-, di- and trisulfide molecules with different spectroscopic signatures as potential basis functions for linear combination analysis. The set of basis functions is chosen after a comparison of the corresponding spectra taken in transmission and fluorescence modes from highly diluted samples. The method of self-absorption corrected linear combination analysis is validated by reliably reproducing the nominal compositions of well-known mixtures with varying sample thicknesses and concentrations. Finally, by the assignment of mono-, di- and trisulfide coefficients to the corresponding NEXAFS spectra, this method is applied to organo-sulfur cathode materials determining the distribution of sulfur strand lengths depending on the sulfur feed ratio in inverse vulcanization.

2 Experimental setup, method and materials

2.1 Sample preparation

Commercially available dipropyl sulfide (DPS), dipropyl disulfide (DPDS) and dimethyl trisulfide (DMTS), see Fig. 1, were used for the validation of the method. The 4 : 1 and 1 : 4 mixtures consist of respective volumetric mixing ratios of DPS and DPDS, while the 2 : 8 : 0, 1 : 8 : 1 and 0 : 8 : 2 samples consist of DPS, DPDS and DMTS in the respective volumetric mixing ratios.

The diluted samples were mixed with *n*-dodecane, with the level of dilution determined by volume. For 1 : 25 dilution, 0.2 ml of the molecular mixture was diluted with 5 ml of *n*-dodecane. From this mixture, 0.4 ml was filled into a coin cell which corresponds to a full cell (infinitely thick sample). Another 5 ml *n*-dodecane was added to the remaining liquid to reach a dilution level of *ca.* 1 : 52 from which again 0.4 ml was filled into another coin cell.

The liquid samples were prepared in coin cells equipped with X-ray transparent and vacuum compatible 12.7 μm thick Kapton windows to use the same experimental setup as in previous studies.[31]

Thin samples were prepared by filling the coin cell with only a droplet of the liquid which moistened the window to form a thin film. Thick samples were achieved by filling the coin cell with 0.4 ml of the liquid.

For the preparation of the S_nNDI_y powder samples *via* inverse vulcanization, elemental sulfur (S_8, sublimated, Grüssing, 99%), allylamine (Acros Organics, 98%), and naphthalene-1,4,5,8-tetracarboxylic dianhydride (TCI, >95%) were used without any further purification. *N*,*N*′-Bis(2-propenyl)-1,4,5,8-naphthalene-tetracarboxylic diimide (NDI-pro)[33] and the S_nNDI_y cathode materials were synthesized following procedures similar to those reported previously.[26] The structure of the S_nNDI_y network is depicted in Fig. 1.

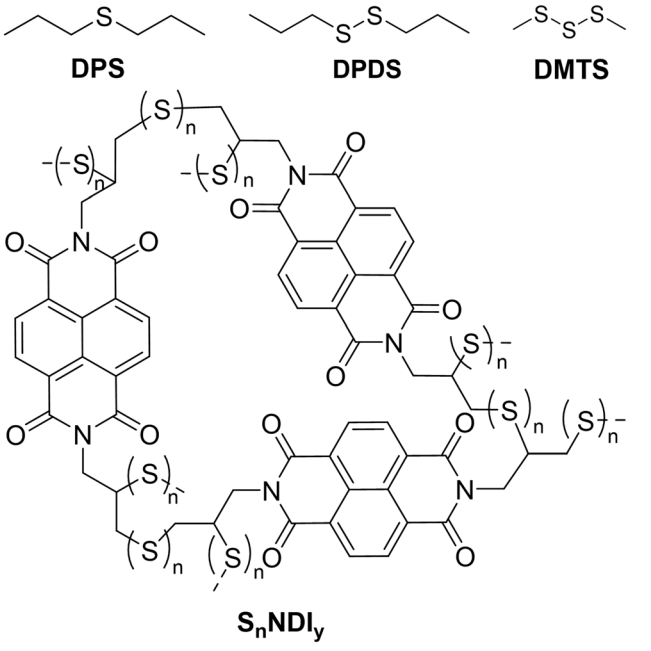

Fig. 1 Chemical structure of the three organosulfur liquids, dipropyl sulfide (DPS), dipropyl disulfide (DPDS) and dimethyl trisulfide (DMTS), used for the basis spectra and the validation of the method, and the S_nNDI_y network of the cathode material.

Table 1 Synthesis parameter and properties of S_nNDI_y powder samples: S_8 and NDI-pro mass and feed weight ratios, stoichiometric sulfur strand length n from feed ratio (n feed), reaction time, yield and Elemental Analysis (EA) results for NDI incorporated weight ratio y and stoichiometric sulfur strand length n

S_nNDI_y	S_8 mass	NDI-pro mass	S_8/NDI-pro feed weight ratio	n feed	Reaction time	Yield	y (EA)	n (EA)
$S_{0.6}NDI_{90}$	0.08 g	0.82 g	9/91	0.5	24 hours	0.43 g (48%)	90	0.6
$S_{1.1}NDI_{83}$	0.16 g	0.84 g	16/84	1.0	7 hours	0.72 g (72%)	83	1.1
$S_{1.5}NDI_{78}$	0.22 g	0.78 g	22/78	1.5	2.5 hours	0.87 g (87%)	78	1.5
$S_{2.2}NDI_{71}$	0.30 g	0.70 g	30/70	2.3	1.5 hours	0.93 g (93%)	71	2.2

For the synthesis of S_nNDI_y powder samples, sulfur and NDI-pro in the masses shown in Table 1 and 1.0 ml of 1-chloronaphthalene were added to an 8 ml vial equipped with a magnetic stir bar. The vial was then capped and placed in a metal heating block at 135 °C. Once the solids had fully dissolved at around 160 °C, stirring at 800 rpm was started and the temperature was raised further to 180 °C within 2–3 minutes. Over time, the viscosity of the reaction solution increased, and after the reaction time specified in Table 1, the mixture solidified, causing the stirring to stop. The reaction was therefore stopped and the reaction mixture cooled to around 50 °C. At this point, methanol (MeOH, 6 ml) was added, and the solids were crushed into smaller pieces. They were then filtered and washed with MeOH several times. The filtered solid was then Soxhlet extracted separately overnight with MeOH, acetone and dichloromethane (for $S_{0.6}NDI_{90}$ and $S_{1.1}NDI_{83}$ only) to remove unreacted NDI-pro. The powder was then dried under vacuum at 60 °C for 24 hours, with the yield of powder indicated in Table 1. According to previous publications, no unreacted sulfur (S_8) was observed in Differential Scanning Calorimetry (DSC) and Thin-Layer Chromatography (TLC) analysis of the S_nNDI_y samples used here.[26]

The grain size in the powder samples was not determined precisely and varied between approximately 1 μm and 1 mm for different compositions. However, the powder samples were prepared including multiple grains to form films with thicknesses of at least 100 μm, corresponding to infinitely thick samples with respect to the self-absorption effect. They have been sticked to Si wafers with carbon glue pads to have the pure powder in the X-ray beam.

2.2 NEXAFS measurements

The NEXAFS measurements in fluorescence mode were performed at the Tender X-ray MicroFocus (MiFo) beamline[34] in the PTB laboratory at BESSY II. The beamline was operated in Double Crystal Monochromator (DCM) mode using Si(111) crystals.

Transmission data, taken from ref. 31, were measured at PTB's Four Crystal Monochromator (FCM) beamline[35] and are shown for comparison.

Due to the data originating from different measurement times at different beamlines, the energy axes differ slightly by approximately 0.5 eV which also represents the uncertainty of the absolute energy calibration of the beamlines. For a meaningful and reasonable comparison of the data, the energy axis of the fluorescence data was aligned with the previously reported transmission data.

As in previous investigations,[31] the experimental setup was optimized for X-ray spectrometric measurements on batteries.[8] The liquid samples were prepared in CR2032 coin cell housings to fit the previously used sample holder in the UHV measurement chamber. The exciting X-ray beam reached the sample through a 12.7 μm thick Kapton window covering a 2 mm-diameter hole in the positive case of the coin cell housing.

The powder samples were attached to a Si wafer which was mounted on the sample holder to manipulate the sample position relative to the X-ray beam.

The NEXAFS signal taken in fluorescence mode was measured using an energy-dispersive silicon drift detector (SDD) which was positioned at an angle of 90 degrees to the incoming beam, while the angle between the sample and the incoming beam and the detected fluorescence radiation was 45 degrees each. The measurements were performed at the sulfur K-edge with the typical S–S peak located at an incident X-ray energy of 2472.1 eV. The SDD was positioned in the plane of the storage ring in order to reduce elastic X-ray scattering. The distance between the SDD and the sample was chosen such that the count rate did not significantly exceed 10 000 counts per second, thus excluding non-linear detector effects. The exposure time was several seconds for each of the slightly more than 100 energy points. Multiple measurements were performed to verify the reproducibility of the results and exclude significant beam damage.

2.3 Computational details on linear combination analysis

Assuming homogeneous samples, the linear combination analysis was performed applying the self-absorption correction which is valid for any sample thickness.[31] All spectra were fitted simultaneously with self-absorption affecting parameters—the dimensionless effective sample thickness t and the matrix contribution to the total X-ray attenuation γ_0—varying for the different measurements. Besides the coefficients of the respective basis spectra representing the contributions of DPS, DPDS and DMTS to the total spectrum, additional fitted parameters account for the shifted energy axes of the different beamlines as well as for normalization.

NEXAFS spectra are typically normalized to the post-edge value which corresponds to the total mass deposition of sulfur which can be translated into the number of sulfur atoms per area. The linear combination analysis is only performed in

a reduced energy region up to 2474.5 eV to separate different species. An additional fit parameter is introduced to account for the correct normalization in the reduced energy range. This enables the future application to *operando* measurements using cells featuring other sulfur species with spectroscopic signatures at higher energies. Note that no background subtraction was performed, neither in the pre-edge nor in the post-edge regions.

The weights used for fitting depend on the statistical uncertainties of the detected fluorescence counts. In the case of liquid molecules, the relative uncertainty for thick samples is typically lower compared to thin samples because of the higher fluorescence count rate. In the normalized spectrum, this lower uncertainty leads to stronger weights for the self-absorption damped spectra in the combined fit. However, less damped spectra of thin samples feature more information regarding the exact speciation of the sample, whereas the spectra of thick samples are mainly used to determine fit parameters linked to the self-absorption correction. Therefore, the weighting of thin and thick samples for the combined fit was balanced when spectra of both thin and thick samples were employed. The weights for the spectra of thin samples were increased such that the total weight of spectra taken from thin and thick samples were equal for the value of the maximum count rate (lowest relative statistical uncertainty).

3 Results

3.1 Choice of the basis set

For the linear combination analysis, a basis set of self-absorption free NEXAFS spectra is needed. The basis set consists of linearly independent spectra of different molecules to analyze their contributions to experimental spectra of samples with unknown composition.

A self-absorption free NEXAFS spectrum can be acquired in one of the following ways. When measured in transmission mode, the attenuation coefficient μ is determined without damping. The measurement of the photo-absorption coefficient τ by fluorescence analysis is self-absorption free for extremely thin or diluted samples. As previously examined,[31] the minimal thickness achieved using undiluted sulfur-containing liquid samples of the molecules DPS, DPDS and DMTS is on an intermediate order of around 1 μm where the spectrum is still significantly affected by the self-absorption effect. Therefore, in this setup, self-absorption free fluorescence spectra can only be recorded for highly diluted samples.

To determine which basis should be used for the linear combination analysis, NEXAFS spectra of DPS, DPDS and DMTS at a 1 : 1000 dilution by volume with *n*-dodecane were recorded in fluorescence mode, and compared to previously reported spectra taken in transmission mode, as shown in Fig. 2.

Although the spectra are consistent in a qualitative way, the subtle deviations are discussed in detail in order to determine the ideal set of basis spectra.

The fluorescence and transmission measurements were conducted at different beamlines using physically distinct samples, including different sample thicknesses. For transmission measurements, the sample needs to be thin to allow the incident beam to transmit through the sample, which is accomplished by a liquid film moistening the HOPG window. The diluted samples used in fluorescence mode allow for self-absorption free spectra even for infinitely thick samples which facilitates sample preparation and handling.

The transmission data were recorded at the FCM beamline with a rather large beam size of approximately 500 μm. The MiFo beamline which was used for fluorescence measurements had a typical focus size of around 20 μm. The energy resolving power of the DCM at the MiFo beamline is slightly lower than that of the FCM, but of a comparable order as both were used with Si(111) crystals and are sufficiently low compared to the natural width of the S K-shell core-hole state of 0.6 eV.

Using the small beam size of the MiFo beamline, fine raster scans over the whole sample measuring the fluorescence intensity at a fixed beamline energy were performed to test the variations of the signal at different positions in the sample. The diluted (and thick) samples distribute uniformly behind the window, which means that the level of dilution is homogeneously distributed over the whole sample, whereas the thin liquid sample films form a heterogeneous thickness distribution.

Comparing the transmission and fluorescence spectra in Fig. 2, the largest deviation across all three molecules is the local minimum in the energy range around 2474.5 eV. For DPDS and DMTS, where the gradient of this minimum is steeper, the fluorescence signal decreases further than in the transmission spectra. This can be a consequence of the heterogeneous liquid film thickness and the large beam size of the FCM. The model of the self-absorption effect is non-linear with respect to sample thickness. Therefore, the NEXAFS spectrum of a sample with significantly varying sample thickness cannot be expressed with this model without treating it in its integral form which would furthermore require the exact thickness distribution.

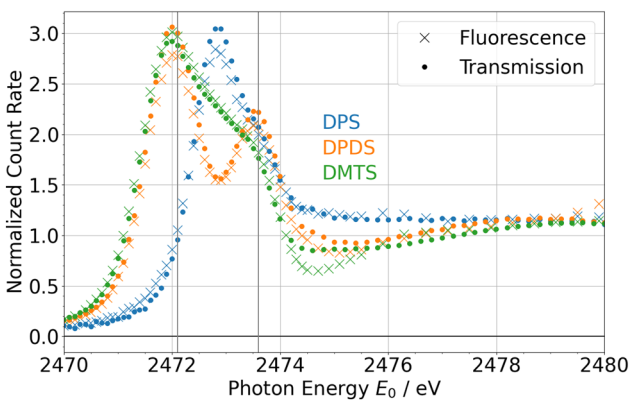

Fig. 2 NEXAFS spectra of DPS (blue), DPDS (orange) and DMTS (green), measured at the MiFo beamline in fluorescence mode (crosses) and at the FCM beamline in transmission mode (dots). Samples measured in fluorescence mode were diluted with *n*-dodecane in a volumetric ratio of 1 : 1000. Samples measured in transmission mode were prepared as thin films. Vertical lines at the resonant peak energies of DPDS at 2472.1 eV and 2473.6 eV are shown in all figures to guide the eye.

Minor deviations between spectra of identical samples free from self-absorption recorded in transmission and fluorescence modes can occur due to factors related to fluorescence such as the relaxation probability of the core-hole state. Keeping this in mind, the main resonances show excellent agreement across the different measurement techniques, with no further systematic deviation exceeding the measurement uncertainties. This confirms that the highly diluted samples measured in fluorescence are not affected significantly by the self-absorption effect. Since the experiments to be evaluated with linear combination analysis were performed in fluorescence mode using the MiFo beamline, the fluorescence spectra of diluted samples were chosen as the basis set.

3.2 Validation employing well-known mixtures

As a validation of the method, linear combination analyses of well-known mixtures of the three molecules forming the basis set were performed. Following the previously presented self-absorption correction routine,[31] this was done for both varying sample thicknesses and levels of dilution.

3.2.1 Variation of sample thicknesses. First, samples with different thicknesses were investigated. The samples were undiluted mixtures of DPS and DPDS in volumetric mixing ratios of 4 : 1 and 1 : 4 respectively, each prepared both as a thin liquid film and as an infinitely thick sample. A sample is considered infinitely thick when less than 1% of the X-ray beam is transmitted through it at an energy above the sulfur K absorption edge. Since the linear combination analysis is sensitive to the molar fraction of sulfur atoms in the different species, the nominal coefficient ratios differ from the volumetric mixing ratios. Although the mixture consisted of only two different molecules, all three basis spectra were used for the linear combination analysis in preparation for application to generally unknown sample compositions of organic sulfur compounds.

Some spectra of the thin liquid films were not reproducible in repeated measurements. Raster scans confirmed that the heterogeneous thickness distribution changed with time or due to beam exposure. It is possible that this also applies to the transmission measurements, but it cannot be investigated at the FCM beamline. However, the fine spatial resolution of the MiFo beamline enabled measurements at sample positions where the thickness did not change between repeated measurements and the presented spectra were therefore reproducible.

Fig. 3 shows the experimental spectra and the linear combination fit results for both sample thicknesses including the respective contributions of the basis spectra for the 4 : 1 mixture as an example. Table 2 shows the nominal and fitted coefficients of the basis spectra for both mixtures.

Using self-absorption correction simultaneously applied to the different sample thicknesses, the shape of the experimental spectra can be reproduced well by the linear combination of basis spectra. Qualitatively, the main resonance at 2473 eV of DPS can be observed, with minor contributions from longer sulfur strands indicated by shoulders on both sides of the peak.

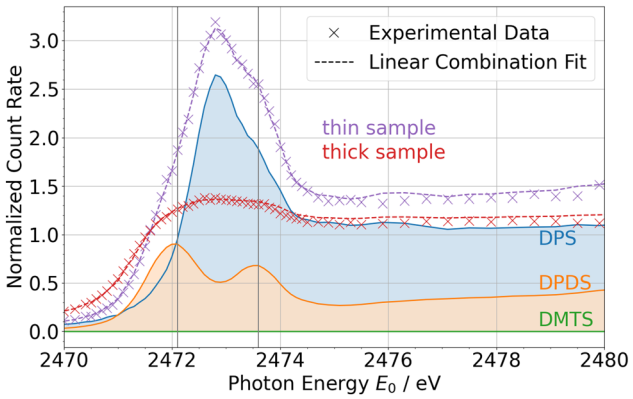

Fig. 3 NEXAFS spectra of an undiluted mixture of DPS and DPDS in a volumetric mixing ratio of 4 : 1, measured at the MiFo beamline in fluorescence mode. Experimentally acquired spectra are shown with crosses; the linear combination fit results are plotted with dashed lines. In the thin sample (purple), the liquid film only moistens the cell window whereas the thick sample (red) is a completely full coin cell. The shape of the spectra and the composition of the sample are reproduced by the linear combination analysis which was performed simultaneously for both different sample thicknesses including self-absorption correction. The contributions of the basis spectra of DPS (blue), DPDS (orange) and DMTS (green) are indicated in their respective colors.

The coefficients extracted by linear combination analysis resemble the nominal contributions well. The largest absolute deviation across both samples and all coefficients is 4% which is within the order of magnitude of the uncertainties. Apart from deviations arising from the fitting routine, model or statistical deviations during the measurements, the composition, solubility and the level of homogeneity of the mixtures potentially lead to this deviation. This means that the lower limit of detection of a certain sulfur species in this analysis is well below 10%. This is sufficient to examine the correlation between the structural (sulfur strand length distribution) and electrochemical (cycle stability and specific capacity) properties of organo-sulfur cathode materials.

Table 2 Nominal and experimentally observed coefficients of the basis spectra for DPS, DPDS and DMTS in the linear combination analysis of thin and thick samples of undiluted 4 : 1 and 1 : 4 mixtures of DPS and DPDS. Since the samples were mixed by volume and the coefficients correspond to the molar fraction of sulfur atoms in respective species, the nominal coefficient ratios differ from the volumetric mixing ratios. The uncertainties given for the nominal coefficients originate from the mixing process whereas the statistical standard uncertainty of the fit is given for the experimental values

Mixture (volume)		Coefficients (molar fraction)		
DPS : DPDS		DPS	DPDS	DMTS
4 : 1	Nominal	69(2)%	31(2)%	0(0)%
	Experimental	73(3)%	27(2)%	0(2)%
1 : 4	Nominal	12(1)%	88(1)%	0(0)%
	Experimental	11(1)%	89(2)%	0(2)%

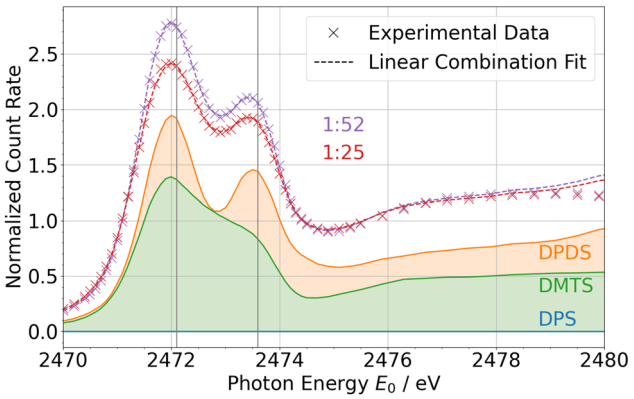

Fig. 4 NEXAFS spectra of a mixture of DPS, DPDS and DMTS in a volumetric mixing ratio of 0 : 8 : 2 (no DPS), measured at the MiFo beamline in fluorescence mode. Experimentally acquired spectra are shown with crosses; the linear combination fit results are plotted with dashed lines. The samples were diluted with *n*-dodecane in ratios of 1 : 25 (red) and *ca.* 1 : 52 (purple). The shape of the spectra and the composition of the sample are reproduced by the linear combination analysis which was performed simultaneously for both different levels of dilution including self-absorption correction. The contributions of the basis spectra of DPS (blue), DPDS (orange) and DMTS (green) are indicated in their respective colours.

As there is no DMTS in the mixtures, the respective coefficient is expected to vanish. This is confirmed by the analysis showing that the DMTS basis spectrum is sufficiently linearly independent from the other basis spectra. Furthermore, it can be expected that absent sulfur species can be identified by the linear combination analysis with deviations smaller than 5%.

3.2.2 Variation of levels of dilution. Similarly, the method of linear combination analysis was validated employing diluted samples. DPS, DPDS and DMTS were mixed in volumetric mixing ratios of 2 : 8 : 0, 1 : 8 : 1 and 0 : 8 : 2 respectively, and then diluted with *n*-dodecane in a ratio of 1 : 25. Coin cells were filled with these diluted samples forming infinitely thick samples.

Additionally, the 0 : 8 : 2 sample was diluted further to a volume ratio of *ca.* 1 : 52 and also filled into a coin cell.

Fig. 4 shows the experimental spectra and the linear combination fit results for both levels of dilution including respective contributions of the basis spectra for the 0 : 8 : 2 mixture as an example. Table 3 shows the nominal and fitted coefficients of the basis spectra for all three mixtures.

Since the diluted samples are infinitely thick, it is sufficient to measure a single level of dilution to determine the γ_0 value of the self-absorption correction during the linear combination analysis as the only free self-absorption related parameter. It increases when DMTS is replaced by DPS because of the decreasing sulfur content. The fitted values for the 1 : 25 diluted samples range from 2.2 (0 : 8 : 2) to 2.6 (1 : 8 : 1) and 3.2 (2 : 8 : 0). The thickness was fitted to be infinitely thick for all samples.

For the 1 : 52 diluted 0 : 8 : 2 sample, γ_0 was fitted to 4.7 which is slightly more than double the value of the 1 : 25 diluted sample. This confirms the physical meaning of γ_0 as a measure of dilution in the sense of matrix contributions to the total X-ray attenuation coefficient.

Table 3 Nominal and experimentally observed coefficients of the basis spectra for DPS, DPDS and DMTS in the linear combination analysis of diluted samples of 2 : 8 : 0, 1 : 8 : 1 and 0 : 8 : 2 mixtures of DPS, DPDS and DMTS. All samples were diluted with *n*-dodecane in a ratio of 1 : 25, whereas 0 : 8 : 2 was additionally measured in a dilution ratio of *ca.* 1 : 52. Since the samples were mixed by volume and the coefficients correspond to the molar fraction of sulfur atoms in respective species, the nominal coefficient ratios differ from the volumetric mixing ratios. The uncertainties given for the nominal coefficients originate from the mixing process whereas the statistical standard uncertainty of the fit is given for the experimental values

Mixture (volume)		Coefficients (molar fraction)		
DPS : DPDS : DMTS		DPS	DPDS	DMTS
2 : 8 : 0	Nominal	12(3)%	88(3)%	0(0)%
	Experimental	11(1)%	87(1)%	2(1)%
1 : 8 : 1	Nominal	5(2)%	74(5)%	21(5)%
	Experimental	4(1)%	68(1)%	28(1)%
0 : 8 : 2	Nominal	0(0)%	64(7)%	36(7)%
	Experimental	0(1)%	60(1)%	40(1)%

The dominance of DPDS can already be seen qualitatively in the spectrum. The levels of dilution correspond to values of ζ of around 5 and 10 in the self-absorption correction, respectively, which means that the spectra are moderately affected by self-absorption damping. The second peak at 2474 eV is less intense than the first peak at 2472 eV compared to the pure DPDS spectrum which suggests a contribution of DMTS. However, potential other contributions and the exact composition ratios cannot be approximated without the quantitative linear combination analysis.

The experimentally acquired coefficients are in good agreement with the nominal values. DMTS coefficients tend to overestimate the contribution of the trisulfide strand with the largest absolute deviation of 7%. The DPS coefficients have the least deviations which suggests that minor monosulfide contributions might be detectable even below 5%. The systematic overestimation of DMTS should be kept in mind when discussing the application of the linear combination analysis to organo-sulfur battery materials, assigning the sulfur strand distribution to a previously unknown sample. However, in the 2 : 8 : 0 sample without DMTS and the 0 : 8 : 2 sample without DPS, the contributions of the absent species were fitted with only up to 2% which confirms that they are identified to be absent by the analysis.

3.3 Distribution of sulfur strand lengths in organo-sulfur cathode materials

After validating the linear combination analysis method using self-absorption free reference spectra of DPS, DPDS and DMTS with mixtures of well-known compositions, including a discussion of the maximum coefficient deviations, it is applied to organo-sulfur cathode materials with varying sulfur loads.

The sulfur feed ratio in the inverse vulcanization of these materials determines the sulfur strand length.[26] By elemental analysis, the incorporated weight ratios of sulfur and the monomer can be determined. These weight ratios can be

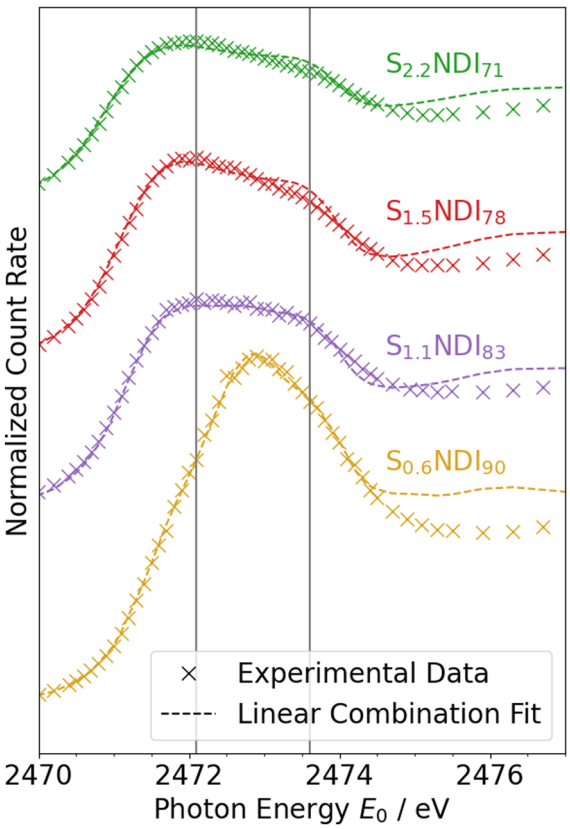

Fig. 5 NEXAFS spectra of organo-sulfur cathode materials S_nNDI_y with varying sulfur loads, measured at the MiFo beamline in fluorescence mode. The linear combination analysis reproduces the shape of the spectra following a sulfur strand length distribution where the average sulfur strand length increases with the sulfur feed ratio.

translated into molar ratios. An NDI-pro monomer has 2 allyl groups where each broken double bond allows 2 sulfur strands to connect, and each sulfur strand connects 2 NDI-pro cross-linker units. Hence, the term "stoichiometric sulfur strand length" n is defined as half the molar ratio of sulfur to NDI-pro to characterize the materials S_nNDI_y. Under the assumption that all allyl groups were broken in order to build sulfur strands and that the created sulfur strands had the same number of atoms, all sulfur strands would have the length n. It is possible that some allyl sites are not accessed by sulfur atoms which leads to less, but longer sulfur strands. The extreme case is that S_8 rings only break once to form sulfur strands of length 8. Thus, different numbers of sulfur strands are built – the higher the stoichiometric strand length, the more strands.

The spectroscopic signatures of DPS, DPDS and DMTS are used to identify components of mono-, di- and trisulfide strands in the organo-sulfur cathode network and subsequently to determine the distribution of sulfur strand lengths.

Powder samples of four organo-sulfur cathode materials S_nNDI_y with different sulfur feed ratios were analyzed regarding the distribution of sulfur strand lengths. In Fig. 5, the experimental spectra are shown together with the linear combination fit results. Table 4 summarizes the respective coefficients for all four samples.

Table 4 Experimentally observed coefficients of the basis spectra for DPS, DPDS and DMTS in the linear combination analysis of organo-sulfur cathode materials with varying sulfur loads. DPS, DPDS and DMTS coefficients represent mono- (S_1), di- (S_2) and trisulfide (S_3) linkages, respectively. The given uncertainties are the statistical standard uncertainties of the fit results

	Coefficients (molar fraction)		
Sample	DPS	DPDS	DMTS
$S_{0.6}NDI_{90}$	77(4)%	8(3)%	14(3)%
$S_{1.1}NDI_{83}$	29(4)%	20(9)%	51(9)%
$S_{1.5}NDI_{78}$	12(2)%	23(4)%	65(5)%
$S_{2.2}NDI_{71}$	9(2)%	23(4)%	68(5)%

Looking at the $S_{0.6}NDI_{90}$ spectrum qualitatively, DPS has a dominating contribution which corresponds to monosulfide strands. It is worth explicitly mentioning that the majority of S–S bonds of an S_8 ring needs to break to form sulfur strands which mainly consist of only one atom each. Following the notation with $n = 0.6$, approximately half of all allyl groups remain either unreacted or homopolymerized. NEXAFS spectra are obtained by measuring the fluorescence signal of sulfur. Therefore, sites of unreacted or homopolymerized NDI-pro (strand length 0, absence of sulfur) are not visible spectroscopically, which makes the measured sulfur strand length distribution systematically higher than the stoichiometric value of $n = 0.6$.

The linear combination analysis assigns coefficients of 77% to DPS, only 8% to DPDS and 14% to DMTS for this sample. Comparing the fitted compositions with the nominal compositions of the well-known mixtures presented in the previous sections, the maximum deviation was estimated to be 7%, with a tendency to overestimate the DMTS contribution. This clearly suggests the predominant existence of monosulfide strands compared to longer sulfur strands with lengths of at least 2. Therefore, the S_8 rings almost completely break down into single sulfur atoms during the inverse vulcanization process. Regarding the application to batteries, these monothioethers are electrochemically inactive which would lead to a battery with low specific capacity.

The $S_{1.1}NDI_{83}$ spectrum barely shows peaks, but rather displays an almost constant plateau between 2472 eV and 2473.5 eV which suggests that different sulfur strand lengths exist to a significant extent. The linear combination analysis confirms this with coefficients of at least 20% for each of the basis molecules. There is still a significant amount of monosulfide strands which is consistent with the stoichiometric sulfur strand length of $n = 1.1$. However, there are more than twice as many sulfur atoms in strands consisting of two or more sulfur atoms. This requires a significant amount of the allyl groups in NDI-pro to remain unreacted, just like in $S_{0.6}NDI_{90}$, while the S–S bonds of S_8 break to form strands of various lengths. It is therefore not possible to design a network with a discrete distribution of sulfur strands with a length of at least 2.

Besides the determined distribution of oligosulfide lengths, the composition obtained from elemental analysis suggests the presence of either unreacted or homopolymerized allyl groups. A small amount of NDI-pro monomer was removed by Soxhlet extraction from $S_{0.6}NDI_{90}$ and $S_{1.1}NDI_{83}$, and unreacted allyl groups were not visible in the solid-state NMR spectra of these two materials. Previously, it was shown that homopolymerization of NDI-pro did not occur using AIBN as the initiator.[26] While we cannot entirely exclude homopolymerization of NDI-pro under the conditions of inverse vulcanization, we conclude that the mismatch of the sulfur strand length distribution from NEXAFS and the stoichiometric value from elemental analysis is likely caused by unreacted NDI-pro.

The cathode powder samples $S_{1.5}NDI_{78}$ and $S_{2.2}NDI_{71}$ give both similar spectra and coefficients. The main difference which is observable qualitatively is the increased self-absorption damping in spectra of the samples with higher sulfur content which corresponds to a higher sulfur load and thus longer sulfur strand lengths. In both these samples, the DPS coefficient drops to less than 15% which means that the breakdown of the S_8 rings into single sulfur atoms becomes less probable for higher sulfur feed ratios. The DMTS coefficients are almost 70%, making it the dominating species even when a systematic overestimation from the validation with the well-known mixtures is taken into account. Since the coefficient describes the molar fractions of the respective species, the number of longer sulfur strands is not as dominant as the coefficients suggest since longer strands consist of more sulfur atoms. However, approximately half of the sulfur strands in $S_{1.5}NDI_{78}$ and more than half of the strands in $S_{2.2}NDI_{71}$ have a length of 3, based on the coefficients.

Comparing the experimentally observed spectra with the linearly combined spectra, there is a qualitative deviation in the peak ratios of the resonances at 2472 eV and 2474 eV. Following de Kock,[30] the first peak at 2472 eV can be assigned to internal sulfur atoms in longer strands with a length of at least 3. This contribution increases with increasing strand length, as the number of internal sulfur atoms in a strand of length m equals $m - 2$. Therefore, it can be assumed that a significant proportion of sulfur strands has a length greater than 3. The spectral signature of internal sulfur atoms in longer sulfur strands is strongly correlated with that of elemental sulfur.[36] Thus, including the spectrum of S_8 into the basis set could improve the quality of the analysis even though elemental sulfur was not observed in the S_nNDI_y samples.

We could not successfully obtain an S_8 spectrum with negligible self-absorption damping for the present study. However, supplying suitable and reliable reference spectra, experimentally or computationally, may enable the quantification of longer strands than 3 or unreacted S_8 rings.

4 Conclusion

It was demonstrated that a reliable quantitative sulfur strand length distribution can be assigned to different organo-sulfur cathode materials made by inverse vulcanization featuring varying sulfur loads. This sulfur strand length distribution is given by the coefficients of a linear combination analysis of X-ray absorption spectra which was performed with a self-absorption correction.

The quantification method was validated by the determination of respective coefficients for mono-, di- and trisulfide strands in various mixtures with well-known compositions of discrete model compounds. The samples were either infinitely thick with varying levels of dilution or highly concentrated with varying intermediate sample thicknesses. The experimental spectra were reproduced by a self-absorption corrected linear combination analysis using self-absorption free basis spectra.

The analysis method was then successfully applied to organo-sulfur cathode materials with varying sulfur loads. Besides providing a quantitative distribution of mono-, di- and trisulfide strands, it could especially be shown that the majority of S_8 rings entirely breaks into single-atom sulfur strands for materials with low sulfur load. With an increasing sulfur feed ratio, the sulfur strand length distribution shifts towards longer strands. There are indications of longer sulfur strands than length 3 in networks with a higher sulfur load. However, they can only be quantified through a modification in the presented method, for example, by using reliable theoretical reference spectra. The distribution of sulfur strands generally remains broad as several sulfur strand lengths occur for a given sulfur load, *i.e.* there is no discrete distribution of sulfur strand lengths achieved with a certain sulfur feed ratio. With this method, it cannot be determined whether NDI-pro remains unreacted or homopolymerizes during the inverse vulcanization.

Since it is possible to quantitatively determine the sulfur strand length distribution, the development of cathode materials with discrete sulfur strand length distributions can be monitored with the presented analysis method. Taking the cycling performance of the examined cathode materials into account,[26] the batteries' performance can be linked to the sulfur strand length distribution and thus an ideal network composition can be proposed. The key parameters of specific capacity and cycle stability, depending on the sulfur strand length distribution can be transferred to any organo-sulfur cathode network and lithium sulfur battery materials universally.

The linear combination analysis forms a prerequisite for further application to *operando* investigations. While other species need to be taken into account, it enables monitoring of how the sulfur strand length distribution inside the cathode network evolves during a cycle and over the course of several cycles. In particular, it can be studied which sulfur strand length is stable during this dynamic electrochemical process.

Furthermore, the analysis method can be extended to numerous applications across the whole NEXAFS community. It can be applied using either experimental or theoretical reference spectra. With a self-absorption correction incorporated, sample thicknesses between infinitely thin (nanometer) and infinitely thick (millimeter, depending on the element of interest) can be assessed for quantitative fluorescence NEXAFS analysis.

Author contributions

KS and HY prepared the liquid samples and RM developed and prepared the powder samples. KS, HY and MM performed the measurements. KS and MM analysed the NEXAFS spectra. MM, MW and MS designed the full project and all authors participated in writing.

Conflicts of interest

There are no conflicts of interest to declare.

Data availability

Data for this article, including all presented experimental NEXAFS spectra taken in fluorescence mode, are available in the Open Access Repository of the Physikalisch-Technische Bundesanstalt (PTB-OAR) at **https://doi.org/10.7795/720.20250710**.[37]

Acknowledgements

We acknowledge funding from the German Research Foundation (DFG) through the Priority Programme "Polymer-based Batteries" (SPP 2248) under project number 441323218.

Notes and references

1 R. Rauh, K. Abraham, G. Pearson, J. Surprenant and S. Brummer, *J. Electrochem. Soc.*, 1979, **126**, 523.
2 P. G. Bruce, S. A. Freunberger, L. J. Hardwick and J.-M. Tarascon, *Nat. Mater.*, 2012, **11**, 19–29.
3 M.-K. Song, E. J. Cairns and Y. Zhang, *Nanoscale*, 2013, **5**, 2186–2204.
4 L. F. Nazar, M. Cuisinier and Q. Pang, *MRS Bull.*, 2014, **39**, 436–442.
5 A. Manthiram, Y. Fu, S.-H. Chung, C. Zu and Y.-S. Su, *Chem. Rev.*, 2014, **114**, 11751–11787.
6 X. Ji and L. F. Nazar, *J. Mater. Chem.*, 2010, **20**, 9821–9826.
7 Y. V. Mikhaylik and J. R. Akridge, *J. Electrochem. Soc.*, 2004, **151**, A1969.
8 C. Zech, P. Hönicke, Y. Kayser, S. Risse, O. Grätz, M. Stamm and B. Beckhoff, *J. Mater. Chem. A*, 2021, **9**, 10231–10239.
9 S. Bai, X. Liu, K. Zhu, S. Wu and H. Zhou, *Nat. Energy*, 2016, **1**, 1–6.
10 Y. Zhang, C. Guo, L. Zhou, X. Yao, Y. Yang, H. Zhuang, Y.-R. Wang, Q. Huang, Y. Chen, S.-L. Li, *et al.*, *Small Sci.*, 2023, **3**, 2300056.
11 K. Liu, H. Zhao, D. Ye and J. Zhang, *Chem. Eng. J.*, 2021, **417**, 129309.
12 R. Matsidik, D. A. Suhagiya, M. H. Goti and M. Sommer, *J. Polym. Sci.*, 2025, **63**, 4640–4648.
13 D. Mecerreyes, N. Casado, I. Villaluenga and M. Forsyth, *Macromolecules*, 2024, **57**, 3013–3025.
14 B. Esser, F. Dolhem, M. Becuwe, P. Poizot, A. Vlad and D. Brandell, *J. Power Sources*, 2021, **482**, 228814.
15 Y. Lu and J. Chen, *Nat. Rev. Chem.*, 2020, **4**, 127–142.
16 T. B. Schon, B. T. McAllister, P.-F. Li and D. S. Seferos, *Chem. Soc. Rev.*, 2016, **45**, 6345–6404.
17 Z. Song and H. Zhou, *Energy Environ. Sci.*, 2013, **6**, 2280–2301.
18 S. Muench, A. Wild, C. Friebe, B. Haupler, T. Janoschka and U. S. Schubert, *Chem. Rev.*, 2016, **116**, 9438–9484.
19 D. Mecerreyes, L. Porcarelli and N. Casado, *Macromol. Chem. Phys.*, 2020, **221**, 1900490.
20 P. Novák, K. Müller, K. Santhanam and O. Haas, *Chem. Rev.*, 1997, **97**, 207–282.
21 X. Jia, Y. Ge, L. Shao, C. Wang and G. G. Wallace, *ACS Sustain. Chem. Eng.*, 2019, **7**, 14321–14340.
22 B. Häupler, R. Burges, C. Friebe, T. Janoschka, D. Schmidt, A. Wild and U. S. Schubert, *Macromol. Rapid Commun.*, 2014, **35**, 1367–1371.
23 S.-R. Deng, L.-B. Kong, G.-Q. Hu, T. Wu, D. Li, Y.-H. Zhou and Z.-Y. Li, *Electrochim. Acta*, 2006, **51**, 2589–2593.
24 Z. Cheng, H. Pan, H. Zhong, Z. Xiao, X. Li and R. Wang, *Adv. Funct. Mater.*, 2018, **28**, 1707597.
25 Z. Pan, D. J. Brett, G. He and I. P. Parkin, *Adv. Energy Mater.*, 2022, **12**, 2103483.
26 R. Matsidik, K. Skudler, S. de Kock, A. Seifert, M. Müller, M. Walter, S. Choudhury and M. Sommer, *ACS Appl. Energy Mater.*, 2023, **6**, 9466–9474.
27 J. Stöhr, *NEXAFS Spectroscopy*, Springer Science & Business Media, 2013, vol. 25.
28 W. Pattanasiriwisawa, J. Siritapetawee, O. Patarapaiboolchai and W. Klysubun, *J. Synchrotron Radiat.*, 2008, **15**, 510–513.
29 K. Shirode, H. Kawai, H. Oe, N. Nakamura and S. Yagi, *e-J. Surf. Sci. Nanotechnol.*, 2020, **18**, 262–267.
30 S. de Kock, K. Skudler, R. Matsidik, M. Sommer, M. Müller and M. Walter, *Phys. Chem. Chem. Phys.*, 2023, **25**, 20395–20404.
31 K. Skudler, M. Walter, M. Sommer and M. Müller, *J. Anal. At. Spectrom.*, 2024, **39**, 2893–2902.
32 T. Penfold, L. Watson, C. Middleton, T. David, S. Verma, T. Pope, J. Kaczmarek and C. Rankine, *Mach. Learn.: Sci. Technol.*, 2024, **5**, 021001.
33 C. Sotiriou-Leventis, Z. Mao and A.-M. M. Rawashdeh, *J. Org. Chem.*, 2000, **65**, 6017–6023.
34 M. Müller, J. Lubeck, M. Krumrey, K. Skudler, H. Yang, T. Gießel, B. Langer, R. Matsidik and A. Sokolov, *Rev. Sci. Instrum.*, 2025, **96**, 091302.
35 M. Krumrey and G. Ulm, *Nucl. Instrum. Methods Phys. Res., Sect. A*, 2001, **467**, 1175–1178.
36 B. Akabayov, C. J. Doonan, I. J. Pickering, G. N. George and I. Sagi, *J. Synchrotron Radiat.*, 2005, **12**, 392–401.
37 K. Skudler, H. Yang, R. Matsidik and M. Müller, *Ex-Situ and Operando NEXAFS Spectra of Organo-Sulfur Compounds*, 2025, **https://oar.ptb.de/resources/show/10.7795/720.20250710**.